





# Enhancing the modal purity of orbital angular momentum photons

Cite as: APL Photonics 5, 070802 (2020); <https://doi.org/10.1063/5.0005597>

Submitted: 23 February 2020 . Accepted: 17 June 2020 . Published Online: 13 July 2020

Isaac Nape , Bereneice Sephton , Yao-Wei Huang, Adam Vallés , Cheng-Wei Qiu , Antonio Ambrosio, Federico Capasso , and Andrew Forbes 



View Online



Export Citation



CrossMark

## ARTICLES YOU MAY BE INTERESTED IN

### Harmonic generation at the nanoscale

Journal of Applied Physics **127**, 230901 (2020); <https://doi.org/10.1063/5.0006093>

### Super-resolution localization microscopy: Toward high throughput, high quality, and low cost

APL Photonics **5**, 060902 (2020); <https://doi.org/10.1063/5.0011731>

### Reconstruction of angle-resolved backscattering through a multimode fiber for cell nuclei and particle size determination

APL Photonics **5**, 076105 (2020); <https://doi.org/10.1063/5.0011500>

additive manufacturing epitaxial crystal growth cerium oxide polishing powder silver nanoparticles sputtering targets III-IV semiconductors CVD precursors europium phosphors

**AMERICAN ELEMENTS**

THE ADVANCED MATERIALS MANUFACTURER®

deposition slugs OLED Lighting spintronics solar energy osmium nanoribbons thin films chalcogenides AuNPs GDC Li-ion battery electrolytes 99.999% ruthenium spheres

endohedral fullerenes copper nanoparticles diamond micropowder CIGS MBE grade materials palladium catalysts flexible electronics beta-barium borate borosilicate glass dysprosium pellets YBCO pyrolytic graphite 3d graphene foam indium tin oxide mesoporous silica raman substrates sapphire windows tungsten carbide InGaAs barium fluoride carbon nanotubes lithium niobate scandium powder

gallium lump glassy carbon nanodispersions InAs wafers laser crystals ultra high purity materials MOFs rare earth metals photovoltaics refractory metals MOCVD organometallics quantum dot superconductors transparent ceramics ultra high purity silicon

American Elements opens up a world of possibilities so you can **Now Invent!**

Over 15,000 certified high purity laboratory chemicals, metals, & advanced materials and a state-of-the-art Research Center. Printable GHS-compliant Safety Data Sheets. Thousands of new products. And much more. All on a secure multi-language "Mobile Responsive" platform.

perovskite crystals yttrium iron garnet alternative energy h-BN gold nanocubes graphene oxide macromolecules photonics rhodium sponge fiber optics beamsplitters infrared dyes zeolites fused quartz metallocenes platinum ink buckyballs Ti-6Al-4V

**Now Invent.™**  
The Next Generation of Material Science Catalogs

[www.americanelements.com](http://www.americanelements.com)



# Enhancing the modal purity of orbital angular momentum photons

Cite as: APL Photon. 5, 070802 (2020); doi: 10.1063/5.0005597

Submitted: 23 February 2020 • Accepted: 17 June 2020 •

Published Online: 13 July 2020



View Online



Export Citation



CrossMark

Isaac Nape,<sup>1</sup> Bereneice Sephton,<sup>1</sup> Yao-Wei Huang,<sup>2,3</sup> Adam Vallés,<sup>1,4</sup> Cheng-Wei Qiu,<sup>3</sup>   
Antonio Ambrosio,<sup>5</sup> Federico Capasso,<sup>2</sup> and Andrew Forbes<sup>1,a)</sup>

## AFFILIATIONS

<sup>1</sup>School of Physics, University of the Witwatersrand, Private Bag 3, Wits, Johannesburg 2050, South Africa

<sup>2</sup>Harvard John A. Paulson School of Engineering and Applied Sciences, Harvard University, Cambridge, Massachusetts 02138, USA

<sup>3</sup>Department of Electrical and Computer Engineering, National University of Singapore, 117583, Singapore

<sup>4</sup>Molecular Chirality Research Center, Chiba University, 1-33 Yayoi-cho, Inage-ku, Chiba 263-8522, Japan

<sup>5</sup>CNST - Fondazione Istituto Italiano di Tecnologia, Via Giovanni Pascoli, 70, 20133 Milano MI, Italy

<sup>a)</sup> Author to whom correspondence should be addressed: [andrew.forbes@wits.ac.za](mailto:andrew.forbes@wits.ac.za)

## ABSTRACT

Orbital angular momentum (OAM) beams with topological charge  $\ell$  are commonly generated and detected by modulating an incoming field with an azimuthal phase profile of the form  $\exp(i\ell\phi)$  by a variety of approaches. This results in unwanted radial modes and reduced power in the desired OAM mode. Here, we show how to enhance the modal purity in the creation and detection of classical OAM beams and in the quantum detection of OAM photons. Classically, we combine holographic and metasurface control to produce high purity OAM modes and show how to detect them with high efficiency, extending the demonstration to the quantum realm with spatial light modulators. We demonstrate ultra-high purity OAM modes in orders as high as  $\ell = 100$  and a doubling of dimensionality in the quantum OAM spectrum from a spontaneous parametric downconversion source. Our work offers a simple route to increase the channel capacity in classical and quantum communication using OAM modes as a basis.

© 2020 Author(s). All article content, except where otherwise noted, is licensed under a Creative Commons Attribution (CC BY) license (<http://creativecommons.org/licenses/by/4.0/>). <https://doi.org/10.1063/5.0005597>

## I. INTRODUCTION

It has been known for at least a century that photons could carry both a spin angular momentum and an orbital angular momentum (OAM), but the “creation” of the latter required rare quadrupole transitions in atoms to occur and so remained largely unstudied. Just over 25 years ago, Allen and co-workers<sup>1</sup> realized that OAM carrying beams could be created in the laboratory using conventional optics in a deterministic manner. They noticed that a phase vortex of the form  $\exp(i\ell\phi)$  would give each photon a “twist” in wavefront, resulting in OAM of  $\ell\hbar$  per photon. Here,  $\phi$  is the azimuthal angle, and  $\ell$  is the helicity or topological charge (an integer), suggesting an optical element with a transmission function in the form of an azimuthally varying phase. Indeed, this was exactly how such beams were first created and detected in both the classical<sup>2,3</sup> and quantum<sup>4</sup> regimes. Since then, the use of azimuthal phase elements for the

creation of such vortex beams has become ubiquitous, implemented by dynamic phase approaches on spatial light modulators (SLMs),<sup>5,6</sup> as well as by geometric phase approaches using liquid crystals<sup>7-9</sup> or metasurfaces (MSs),<sup>10</sup> and has been pioneered to harness the radial degree of freedom by merging these approaches in a single element.<sup>11,12</sup> These phase-only vortex beams have found a myriad of applications, making them highly topical forms of structured light.<sup>13-15</sup>

Although OAM modes can be detected by a suitable conformal mapping in so-called mode sorters,<sup>16</sup> the standard approach is to exploit the reciprocity of light and run the creation step in reverse, e.g., by intensity or phase flattening approaches.<sup>17</sup> Both work on the idea of unraveling the twisted wavefront of the OAM mode and then coupling the Gaussian-like beam into a single mode fiber (SMF) or measuring with a single pixel. Now, although the early successes with these approaches set the stage for further study and

application of OAM beams, the azimuthal phase approach to their creation and detection has some inherent inefficiencies: transverse solutions to the wave equation are 2D structures (in the paraxial limit) so that two indices are needed to describe them, both requiring control in the creation and detection steps. A consequence of using the azimuthal phase alone is that the radial mode content has been ignored, resulting in hypergeometric modes<sup>18</sup> with the desired  $p = 0$  OAM mode having its power distributed across many radial modes.<sup>19</sup> This has deleterious effects for both radial mode purity as well as creation and detection efficiency. While the creation can be dealt with by intra-cavity OAM approaches, which result in pure modes,<sup>20,21</sup> this does not address the detection issue nor the application to quantum states. It may be noted that reference to purity throughout this paper refers to the radial mode purity, i.e., how much power is in, or detected in, the  $p = 0$  OAM mode.

While the effects of radial purity are low for small OAM charges, it becomes increasingly prominent for higher values with several approaches readily achieving high charges of  $\ell = 100$  and beyond using liquid crystal q-plates,<sup>22</sup> spiral phase plate mirrors,<sup>23</sup> anisotropic diffractive waveplates,<sup>24</sup> and others in the phase-only regime. Moreover, due to applications such as working toward testing quantum foundations<sup>23,25</sup> and creating sensitive photonic polarization gears<sup>22</sup> now require higher OAM modes, it follows that the consequential purity is no longer negligible. Here, we pay attention to complex amplitude detection of these modes and show that adjusting the scale in the detection step can be used for enhanced detection efficiencies. Advantages are shown both classically and quantum mechanically. Reciprocally, we also demonstrate the creation of high purity OAM modes with complete azimuthal phase and radial mode control, thus creating a comprehensive approach to working with phase-only generation devices.

To make clear that the solution is not device specific, we employ two fundamentally different phase-only devices with a metasurface enhanced with holographically programmed dynamic phase to produce ultra-high purity classical OAM modes and a SLM-only solution in the quantum realm. The metasurface comprises nano-structured rods patterned for complete control of the OAM state of light, vector and scalar, while the hologram written to a spatial light modulator uses a dynamic phase to introduce complex amplitude modulation, thus engineering all degrees of freedom of the field. Moreover, the scheme is extendable to any OAM encoding device, not limited to SLMs or metasurfaces. Our results will be of particular benefit to both the classical and quantum communication where a large alphabet with a good signal-to-noise ratio is essential.

## II. BACKGROUND

Here, we illustrate the concept of enhancing the creation and detection of high purity OAM modes external to a laser, having already shown that it is possible directly from the source.<sup>21</sup> Importantly, we provide the full details for the classical case and introduce a new quantum case for the enhanced purity of single photons and quantum states. The objective is to reduce the contribution of unwanted radial modes and to concentrate all the energy into the zero order radial mode, both at the creation and detection steps. But how to achieve this in a generic manner? To demonstrate this,

we create high purity OAM modes in the Laguerre–Gaussian basis (natural OAM basis). Such transverse modes,  $\psi_{p,\ell}(r, \phi; w_0)$ , of radial order  $p$  and azimuthal index  $\ell$  are solutions to the wave equation in quadratic index media, including free-space and graded index fiber. The OAM content of the beam is associated with the azimuthal phase,  $\exp(i\ell\phi)$ , while  $w_0$  is a scale parameter, sometimes referred to as the embedded Gaussian beam size. A pure OAM mode in this basis, the mode we desire, would have no radial modes ( $p = 0$ ) and is described by

$$\psi_{0,\ell}(r, \phi; w_0) \propto \left(\frac{r\sqrt{2}}{w_0}\right)^{|\ell|} \exp\left(-\frac{r^2}{w_0^2}\right) \exp(-i\ell\phi). \quad (1)$$

Note that  $\ell$  appears in both the amplitude and phase terms so that both the amplitude and phase modulation are required to produce a true OAM mode in this basis. In fact, it is the amplitude term that results in the intensity null so often associated with such modes. Yet, the conventional approach to producing OAM modes is to approximate this by phase-only azimuthal modulation of a Gaussian beam, as shown in Fig. 1(a), resulting in

$$\tilde{\psi}_\ell(r, \phi; w_0) \approx \exp\left(-\frac{r^2}{w_0^2}\right) \exp(-i\ell\phi). \quad (2)$$

This vortex beam results in the generation of many radial modes, shown in Fig. 1(b), with low power content in the desired  $p = 0$  mode. In fact, the modal powers for all  $p$  and a given  $\ell$  can be expressed as

$$|c_{p\ell}|^2 = \frac{(p + |\ell|)!}{p!} \left| \frac{\Gamma(p + \frac{|\ell|}{2})\Gamma(\frac{|\ell|}{2} + 1)}{\Gamma(\frac{|\ell|}{2})\Gamma(p + |\ell| + 1)} \right|^2. \quad (3)$$

Here, we propose how to overcome this in two approaches: one for creation and the other for detection.

For detection, we observe that the OAM mode scales with the embedded Gaussian beam size ( $w_0$ ). It has been traditional to use this scale in the detection since, by reciprocity, this is the scale at which the vortex beam was initially created. However, ideal ( $p = 0$ ) OAM modes would have a second moment radius of  $w_\ell = w_0\sqrt{|\ell| + 1}$  that corresponds to an intensity ring of radius  $w_0\sqrt{\ell/2}$ . This highlights that while the scale of the final OAM mode will certainly depend on  $w_0$ , it will not be equal to it. We select an optimal scale for the detection in order to maximize modal power in the desired  $p = 0$  mode when the initial mode is *not* amplitude modulated [shown in Eq. (2) and depicted in Fig. 1(a)]. In the case where a mode generated without amplitude modulation is detected with a system that assumes a scale of  $w_0$ , the measured power in the desired  $p = 0$  mode approaches zero as the azimuthal index increases (see the [supplementary material](#)). This case would represent the usual method of detection, particularly in quantum experiments with OAM. For example, an input vortex mode of  $\ell = 1$  at this scale has only about 80% of its energy in the  $\psi_{0,1}$  mode, with the rest spread across higher radial modes. Furthermore, an input vortex mode of  $\ell = 10$  has less than 1% of its energy in the  $\psi_{0,10}$  mode. This places severe limits on the available alphabet using OAM as a basis. We ask what should the  $\ell$  dependent scale parameter be such that the expansion has the minimum power in the unwanted radial modes,  $p \neq 0$ . The salient point is that higher modal power is physically available, but the detection

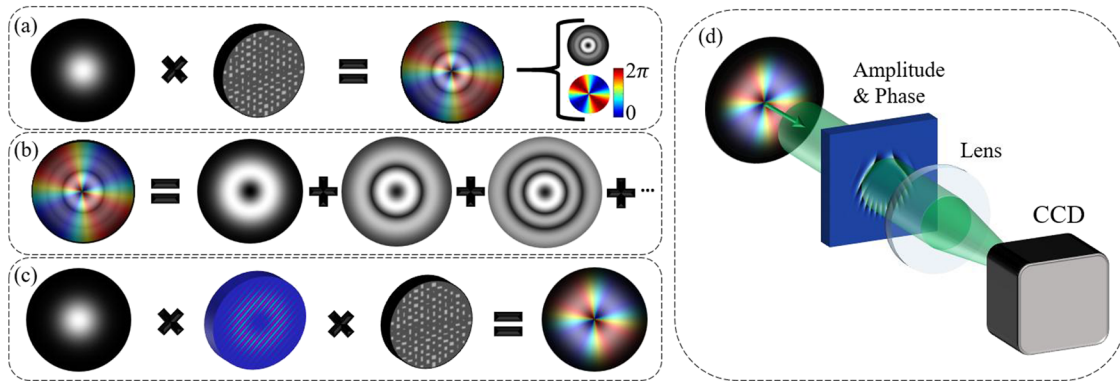


**FIG. 1.** (a) A Gaussian beam modulated by an azimuthal phase, shown here as a metasurface, results in an OAM mode with many radial orders, shown in (b) as the sum of beams with several intensity rings. By combining phase control using holograms and metasurfaces, high purity OAM modes can be produced, as seen in (c). For detection of the modal composition of a beam, conjugate modulation of the mode being evaluated is applied, and the Fourier plane on-axis intensity is measured, as shown in (d).

system needs to be optimized to recover it. Accordingly, we exploit the fact that changing the scale in size-dependent bases can alter the detected modal content.<sup>26</sup> Here, the correct scale to achieve this can be expressed analytically as

$$w_{\text{opt}} = \frac{w_0}{\sqrt{|\ell| + 1}}, \quad (4)$$

leading to an optimized modal power content in the  $p = 0$  mode given by

$$|c_\ell(\alpha_{\text{opt}})|^2 = \left| \frac{2^{\frac{|\ell|}{2}} |\ell| \alpha_{\text{opt}} \Gamma\left(\frac{|\ell|}{2}\right)}{(1 + \alpha_{\text{opt}}^2)^{\left(\frac{|\ell|}{2} + 1\right)} \sqrt{\Gamma(|\ell| + 1)}} \right|^2 \quad (5)$$

when

$$\alpha_{\text{opt}} = \frac{1}{\sqrt{|\ell| + 1}}. \quad (6)$$

The implication of this is best visualized in a quantum experiment where the experimenter has full control over the detection steps but often little control over the creation steps. Rather than detecting for an incoming mode size of  $w_0$ , the detection system should be adjusted to a scale of  $w_{\text{opt}}$ . The prediction is a signal enhancement for a larger available alphabet of OAM modes.

While detection is enhanced by optimizing the available signal with  $w_{\text{opt}}$ , one cannot recover it to 100% as the vortex beam in Eq. (2) is not the desired mode. Amplitude modulation is needed. To illustrate this, we use metasurfaces to create OAM modes of very high order and then circumvent the spread of power into higher order radial modes by employing holographically encoded complex amplitude modulation to correct for the missing amplitude term. By combining a metasurface for azimuthal phase control with high fidelity (since the vortex can be very well defined at the nano-scale) with holographic complex amplitude modulation, we are able to demonstrate ultra-high purity OAM states, even at very high OAM, as given by Eq. (1), with all the power in the  $p = 0$  mode, illustrated in Fig. 1(c). Here, the creation step is summarized that, when reversed,

allows a detection route for the enhanced signal over conventional approaches, as illustrated in Fig. 1(d).

Finally, in the quantum case, the situation is a little different. There is no “initial” beam but only what one detects, which is related to a pseudo initial beam in the form of the pump mode at the crystal. Assuming that the pump is Gaussian and the detection includes single mode fibers (the ubiquitous case), we derive the modal powers to be given by

$$|c_\ell(\alpha_{\text{opt}})|^2 = \left| \frac{2^{\frac{|\ell|+3}{2}} \sqrt{\frac{1}{|\ell|!}} \Gamma\left(\frac{|\ell|}{2} + 1\right) \left(\frac{1}{\alpha_{\text{opt}}^2} + \frac{1}{\eta^2} + 2\right)^{-\left(\frac{|\ell|}{2} + 1\right)}}{\pi^{3/2} w_0^2 \eta \alpha_{\text{opt}}^{|\ell|+1}} \right|^2, \quad (7)$$

with

$$\alpha_{\text{opt}} = \frac{\eta}{\sqrt{(2\eta^2 + 1)(|\ell| + 1)}}, \quad (8)$$

where  $\eta = \frac{w_p}{w_0}$  is the pump field and fiber mode size ratio. This equation can easily be generalized to other pump geometries and detection modalities.

### III. EXPERIMENTAL

#### A. The dielectric metasurface

The metasurface device used for the creation of the classical OAM modes was a dielectric metasurface made of amorphous TiO<sub>2</sub> nano-posts with a rectangular section [the inset of Fig. 2(a)] on a quartz substrate. Each post has a height of 600 nm, while the width and length ( $w_x$ ,  $w_y$ ) change in order to impart a different phase delay to the propagating visible light at 532 nm. More specifically, each nano-post imparts an overall phase delay  $\delta$  to the propagating light and a phase delay difference  $\Delta\chi$  between the field  $x$  and  $y$  components. This last term only depends upon the shape of the post and is called the *form birefringence*: symmetric sections such as squares or circles do not show the form birefringence. Note that amorphous TiO<sub>2</sub> used for these nano-structures is not optically birefringent at this



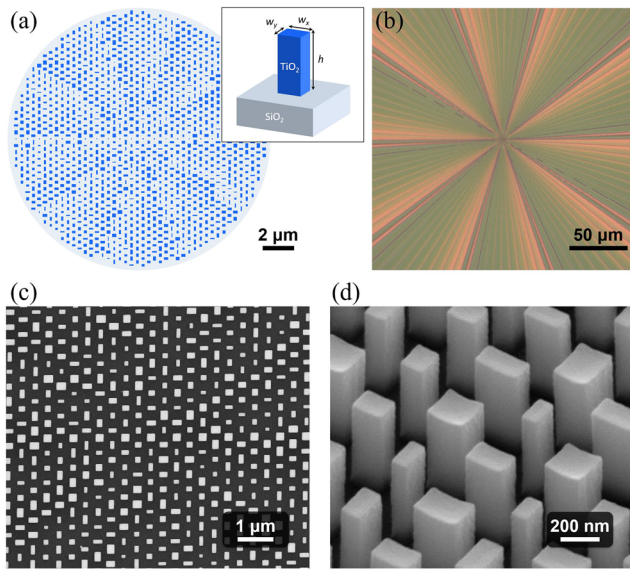


**FIG. 2.** (a) Schematic of a J-plate design. The J-plate imprints two kinds of helical phase profiles for  $x$ - and  $y$ -incident polarization, resulting in output beams with the orbital angular momentum  $m\hbar$  and  $n\hbar$ , where  $m$  and  $n$  can be any independent integers. The metasurface elements are rectangular nano-posts made of amorphous  $\text{TiO}_2$  with a fixed height of  $h = 600$  nm. By changing the width along the  $x$ - and  $y$ -direction ( $w_x$  and  $w_y$ ), the nano-posts impart phase delays given by  $\delta_x$  and  $\delta_y$ . Optical micrographs (b) and scanning electron micrographs (SEMs) [(c) and (d)] of a representative J-plate with the OAM number  $(m, n) = (10, 100)$ . The SEMs show a top view (c) and angled view (d) of the device center.

wavelength. Our metasurface combines both the propagation phase and PB-phase to convert any two orthogonal polarization states of the incident light into the conjugate helical modes with any arbitrary value of orbital angular momentum  $m$  and  $n$ , not just opposite values. This is possible by controlling the PB-phase, the overall phase, and the form birefringence of each element.

Figure 2(a) shows the schematic image of the central part of a representative J-plate that converts two orthogonal linear polarization states (with the field oriented along  $x$  and  $y$ , respectively) into helical modes with the same polarization state and orbital angular momentum  $(m, n) = (10, 100)$ . Figure 2(b) shows an optical microscope image of a J-plate producing helical modes with the orbital angular momentum 10 and 100 for the  $x$ - and  $y$ -linearly polarized incident light, respectively. Figures 2(c) and 2(d) show the scanning electron micrographs (SEMs) of the realized device. Note that the nano-posts have different shapes and orientations to implement the necessary phase gradient. The J-plate is fabricated using electron-beam lithography, followed by atomic layer deposition and etching. Note that the implemented azimuthal phase gradient is visible in the optical image of the device as color variation. In fact, nano-posts with different shapes have different scattering resonance frequencies, resulting in a colorful optical image. For instance, in Fig. 2(b), it is easy to distinguish 10 sectors, each made of 10 inner sectors. This means that for the helical mode resulting from the incident  $y$ -polarized light, in order to

generate a beam with the orbital angular momentum 100, a  $2\pi$  azimuthal phase variation must be accumulated in an angle of just  $2\pi/100$  ( $3.6^\circ$ ).

It is worth noting that the high azimuthal gradient necessary to impart a topological charge (100) to a propagating beam can be realized by means of SLMs. However, the typical pitch of such device is about  $8 \mu\text{m}$ . In our metasurfaces, the unit cell dimension is  $420$  nm that represents a 20 times increase in resolution with respect to a SLM, crucial for high quality vortices. Moreover, a SLM does not affect the light polarization and cannot be used alone to encode spin-to-orbital angular momentum devices. Thus, we elect to use this metasurface approach because the azimuthal phase is well defined down to nano-meter scales for high quality azimuthal OAM modes. This allows us to emphasize the point that while the creation element is as ideal as can be, the purity of the resulting modes is nevertheless very low. It follows that while this work could be implemented with any phase-only device such as spiral phase plates or only a SLM (which is the case in the quantum experiment), we elect to employ the metasurface in the classical

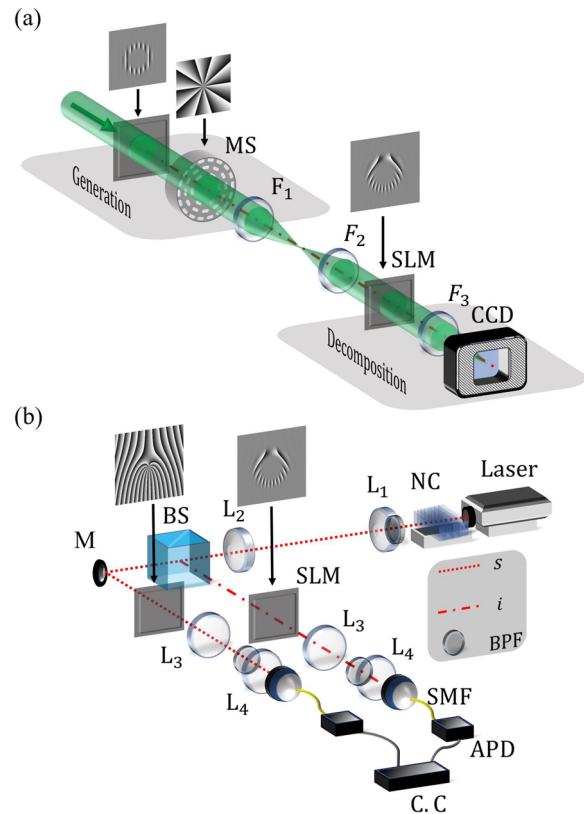


**FIG. 3.** Illustrations of the (a) classical and (b) quantum experimental setups. SLM: spatial light modulator functioning in the reflective mode but drawn here as transmissive; F, L: lens; CCD: charge-coupled device; NC: nonlinear crystal; BS: beam splitter; M: mirror; SMF: single mode fiber; APD: avalanche photodiode; BPF: bandpass filter; s: signal; i: idler; C.C.: coincidence counter, and MS: metasurface. Overhead insets show representative phase maps for the respective beam manipulations carried out at each point.

case. The issue here is in the physics of the situation and not its implementation.

## B. Enhanced generation scheme

To test the concept of enhanced purity in the creation and the enhanced signal in the detection, we used the experimental setups shown in Figs. 3(a) and 3(b) for classical and quantum light, respectively. In the classical experiment, a 532 nm wavelength horizontally polarized laser beam was generated through the phase and amplitude modulation on a HOLOEYE PLUTO spatial light modulator (SLM), allowing one to obtain any desired beam size and phase. The resulting mode traversed the metasurface (MS), which was further relayed with a 4f system ( $F_1$  and  $F_2$  with focal lengths of 200 mm) onto another SLM for analysis. The measurement was performed by detecting the on-axis intensity in the Fourier plane of the second SLM ( $F_3$  with a focal length of 300 mm), yielding the modal spectrum (see modal decomposition in the supplementary material). Phase plots above the optical elements in Fig. 3(a) exemplify the phase transformations imparted to the beam for amplitude correction of the MS and subsequent analysis thereof.

## C. Enhanced two photon detection scheme

The setup used for measurements on the entangled photons is illustrated in Fig. 3(b). Our type I PPKTP crystals produced collinearly propagating photon pairs entangled in the OAM degree of freedom at 810 nm (see the supplementary material). The photon pairs were separated, in path, using a 50:50 beam splitter (BS). From the crystal plane, each pair was imaged onto a SLM with a 4f system ( $L_1$  and  $L_2$  having focal lengths of 100 mm and 500 mm each)

and subsequently imaged ( $L_3$  and  $L_4$  having focal lengths of 750 mm and 2 mm each) into single mode fibers (SMF) for detection with APDs. The photons from each arm were correlated in time using a coincidence counter (C.C.) with a 25 ns coincidence window. All measurements were obtained by recording the photons with an integration time of 5 s. A fixed ratio between the mode fiber radius ( $w_0$ ) of the SMF and the pump photon of  $\eta = 1.5$  was used during the experiment.

## IV. RESULTS

### A. Enhanced generation of OAM modes

In Figs. 4(a) and 4(b), we compute the predicted radial modal power weighing ( $|c_p|^2$ ) for  $\ell = 10$  and  $\ell = 1$  beams, respectively, as a function of ratio,  $\alpha = w_\ell/w_0$ . Accordingly, in each case, the beam waist size is varied on the projection hologram for the detection of each radial mode ranging from  $p = 0$  to  $p = 10$ . Our aim is to engineer the mode by the metasurface and holographic control to produce  $|c_0|^2 \rightarrow 1$ , i.e., 100% of the power in the desired OAM mode in order to emphasize the effect of amplitude control in the generation process. We observe that if no initial amplitude control of the mode is performed and the traditional scale is used ( $w_\ell = w_0$ ) in the detection, then  $|c_0|^2 \approx 0.8$  ( $\ell = 1$ ) and  $|c_0|^2 \approx 10^{-3}$  ( $\ell = 10$ ). This is confirmed by the experiment: the panels shown in (i) for both  $\ell = 1$  and  $\ell = 10$  modes show that the measured power in the radial modes is as predicted by theory. The blue bars represent the experimental data, and the black dots represent the theory. For example, the cross section highlighted by the gray panel at  $w_\ell = w_0$  in the theory plot of Fig. 4(a) is shown again in associated panel (i) as black dots (theory) with experimental data as blue bars. The measured power is spread across many unwanted radial modes, as predicted. There is

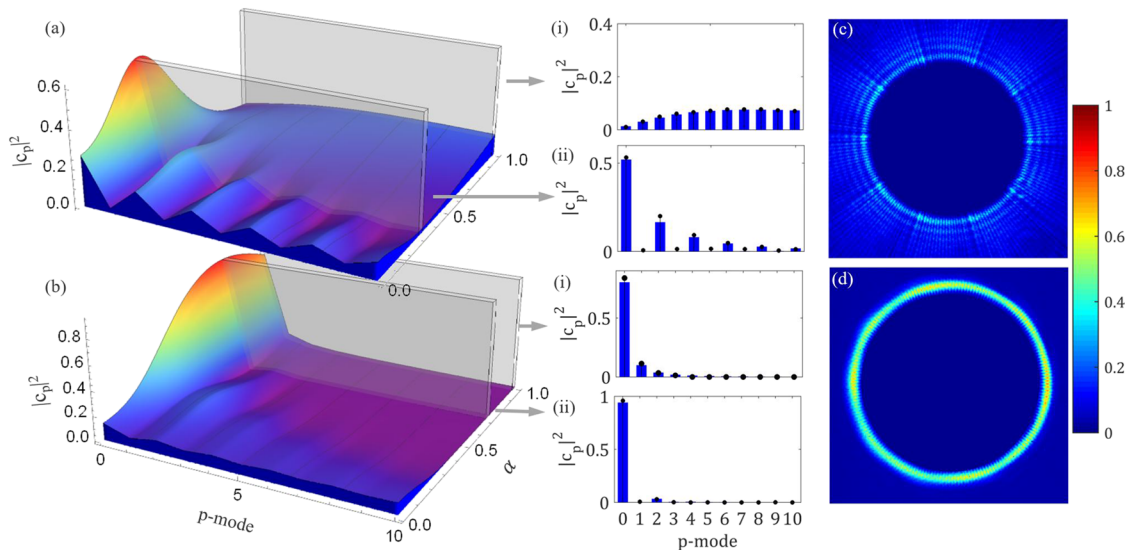


**FIG. 4.** Normalized detection probabilities with variation in the  $p$ -mode index and  $\alpha = w_\ell/w_0$  for (a)  $\ell = 10$  and (b)  $\ell = 1$ . Measured  $p$ -mode spectra (blue bars) are given for detection with (i) the unadjusted mode size ( $w_\ell = w_0$ ) and (ii) the optimal encoded mode size ( $w_\ell = w_{\text{opt}}$ ) shown with the theoretical predictions (black dots). The normalization was performed with respect to the  $p$ -mode distribution. False color map images of an  $\ell = 100$  generated beam with (c) phase-only modulation and (d) amplitude corrected phase modulation are shown.

a second cross section highlighted by the gray panel at  $w_{\text{opt}}$ , corresponding to the peak in the theory plot of Fig. 4(a). The associated panel is in part (ii), again shown as black dots (theory) with experimental data as blue bars. Now, the power in the  $p = 0$  mode has substantially increased from  $<1\%$  to about 50%. This confirms that optimizing the scale at the detection results in significant signal-to-noise enhancements, crucial for optical communication with OAM modes. The same trend is seen in (b) with its associated panels (i) and (ii), again with excellent agreement between theory and experiment. A decrease in the ratio  $\alpha$  also results in an oscillation in the modal power as a function of radial index, with no power in the odd  $p$  modes. This truncated radial mode expansion becomes more evident as the scale outdistances  $w_0$  due to the  $p$  parameter restriction ( $p/2 \in \mathbb{N}$ ) when describing the resulting mode in the LG basis, as theoretically predicted.<sup>27</sup>

So far, only the detection step has been optimized. Next, we wish to apply full amplitude and phase control with our holographically enhanced metasurfaces. To do so, we structure the amplitude only and pass the modified profile through the metasurface to impart the phase profile, akin to the method used by Ref. 28 and in a similar concept in the considerations of Refs. 29 and 30. The results for the two beams are discussed here and shown in Fig. 5(a)

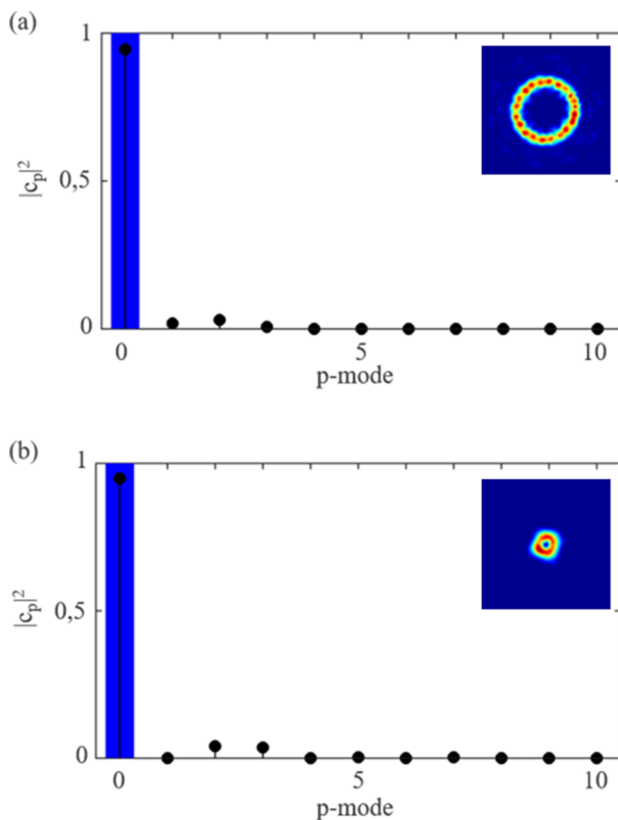


**FIG. 5.** The  $p$ -mode spectrum when full amplitude and phase control is applied for (a)  $\ell = 10$  and (b)  $\ell = 1$ . The bars represent the theory, while the points represent the experiment. Insets show the processed transverse spatial distributions. The small intensity oscillations are due to the metasurface fins.

for  $\ell = 10$  and Fig. 5(b) for  $\ell = 1$ . The modal purity is as close to 100% as we can determine within experimental uncertainty: all the power is now in the desired  $\ell$  with the  $p = 0$  mode, quantitatively characterized by  $|c_0|^2$ . Using  $\ell = 10$  as an example, the initial modal power following traditional schemes was  $|c_0|^2 \approx 4 \times 10^{-3}$ , becoming  $|c_0|^2 = 0.5$  after detection optimization, and  $|c_0|^2 \approx 1$  after full mode control. This represents about a 125 $\times$  and 250 $\times$  signal enhancement. The impact of our approach becomes more enhanced with an increase in  $\ell$ . To illustrate this, we perform these experiments with a metasurface to produce  $\ell = 100$  modes (the highest reported to date by metasurface and metamaterials). Figure. 4(c) shows such a beam created by only modulating the phase, while (d) shows the same beam but produced by our metasurface together with complex amplitude modulation. Even visually, one can see the numerous rings in (c), which “collapse” into a single ring in (d): a high purity OAM mode with an astonishing power enhancement in the desired mode. It is pertinent to point out that *all* phase-only approaches that only modulate a Gaussian beam by an azimuthal phase will produce the rings seen in (c) and is not a factor of the device efficiency. In most reports, the rings are removed by optical filtering prior to recording and hence resulting in unwanted losses.

## B. Enhanced quantum detection of OAM modes

The aforementioned tests modulated and detected classical light fields. To complement the classical results, we also perform a quantum experiment, as shown in Fig. 3(b). It may be noted that while the modes  $(\ell, p)$  are discrete, surface plots were used as a guide so that the trend is easily seen [similar to the lines in Fig. 6(f)], and thus, the discrete values are interpolated to yield the graphs. Here, entangled photons were created using a PPKTP crystal via spontaneous parametric down-conversion (SPDC). Each of the entangled bi-photons were relay imaged to projective optics, with one set projecting onto a vortex state by an azimuthal phase profile, and the other performing full  $\ell$  control of both the amplitude and the phase. This is the quantum equivalent of the classical prepare and measure experiment already reported in Sec. IV A. However, as is customary in such quantum experiments, the detection system includes a single mode fiber so that only the  $p = 0$  mode can be filtered out. Figure 6(a) shows the experimental results for measuring the OAM spiral bandwidth as a function of the scale in the detection ( $\alpha = w_\ell/w_0$ ), with the corresponding theoretical plot shown in (b). Clearly, they are in excellent agreement. Cross sections of the power in a specific  $\ell$  mode, quantified by  $|c_\ell|^2$ , as a function of changing the scale  $\alpha$ , are shown in (c)–(e) for  $\ell = 1, 2$ , and 5, respectively. The theory (black dots) is in good agreement with the experimental data (blue bars). This confirms that the concept we have outlined is equally impactful with quantum light. We predict and observe that the coincidence rate can be dramatically increased by our approach, resulting in a visible spiral bandwidth beyond that possible without scale adjustment: the Schmidt number more than doubles from  $K = 3$  to  $K = 7$ , as shown in Fig. 6(f), demonstrating more than a doubling of the quantum dimensionality. This represents a significant increase in the available dimensions in our OAM Hilbert space and is a consequence of transferring power into the desired mode, thus lifting it from the noise. This experiment also serves to illustrate that it is not the *manner* of implementing the azimuthal phase

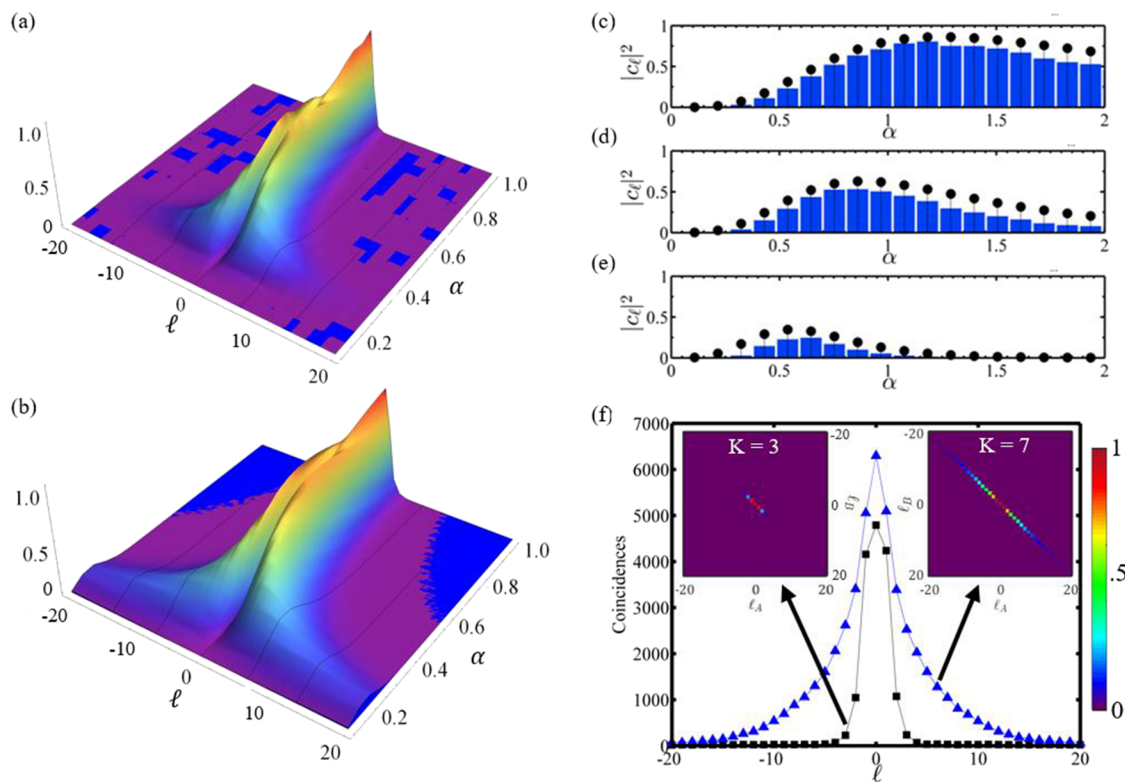


**FIG. 6.** (a) Experimental and (b) simulated coincidence measurements based on the detection probabilities of OAM photons measured with the encoded holograms. (c) The normalized coincidences as a function of  $\alpha = w_\ell/w_0$  for (c)  $\ell = 1$ , (d)  $\ell = 2$ , and (e)  $\ell = 5$ . The bars represent the experimental data, while the points represent the simulation. (f) Spiral-bandwidth plots obtained from the diagonal of the inset mode projections for (left)  $w_0$  and (right)  $w_{\text{opt}}$ . Insets are density plots representing measured coincidences for OAM projections on the SLMs when the encoded LG beam size is  $w_0$  (black squares) and the optimal mode size is ( $w_{\text{opt}}$ ) (blue triangles). Each data point was measured over a 5 s time interval.

pattern that matters—here, only SLMs were used due to the unsuitability of the metasurface for the quantum photon wavelengths. For completeness, we point out that we have not tested the quantum correlations in the new subspaces and so make no statements on the entanglement. However, since the SPDC process produces pure states,<sup>31–35</sup> the full quantum toolkit can be applied to the new subspaces revealed from the noise, including testing for entanglement in high-dimensions.<sup>36</sup>

## V. DISCUSSION AND CONCLUSION

In many applications, the detection of OAM modes implicitly assumes a projection onto a Gaussian-like mode ( $p \approx 0$ ), by coupling into single mode fibers, by OAM mode sorting, or by the match filters used in MUX/DEMUX optical communication systems. In such cases, the detection approach we outlined here will yield an improved signal-to-noise ratio and thus a larger available alphabet, as we have demonstrated with both the classical and quantum states. For completeness, we point out that if the application and/or detection simply integrates out the radial modes, e.g., accumulates all power from a particular azimuthal mode, then there will be neither a gain nor a loss from our approach.

We employed the metasurface in the classical experiment as an example of a phase-only device, which we note could have been replaced with any equivalent element to illustrate our concept. For example, a second SLM could have achieved the same outcome, and this, in fact, was demonstrated with the quantum experiment. Here, a contrast in features between these two devices explicitly emphasizes the generality of the effect and thus universality of how our optimization may be of benefit. The choice of the metasurface allowed us to simply demonstrate a high OAM charge ( $\ell = 100$ ) with a good purity, which was easily achievable with the greater resolution. Additionally, due to the asymmetrical nature of the coupling in the device paired with the amplitude and phase control, which were achieved in separate steps, it would be possible to extend this to easily produce arbitrary high purity vector modes in line with Ref. 28. It may also be interesting to consider the combination of both techniques into a single integrated device in future studies, similar to that achieved by Refs. 11 and 12 or potentially employing phase correction approaches<sup>37,38</sup> for enhanced purity in all degrees of freedom.

In conclusion, we have outlined a simple approach for increasing the detection efficiency of classical and quantum experiments with OAM modes by a simple adjustment of the scale at which



the measurements are made. In the quantum case, this is all that is needed since there is no “initial” mode: the state is determined by the measurement and has no reality prior to that. In the classical case, to truly maximize the signal requires very high purity initial modes. We used metasurfaces that are holographically enhanced to control both the azimuthal and radial profiles of OAM modes to create high purity OAM beams up to  $\ell = 100$ . This applied research paper will be important to applications that seek to exploit OAM as a basis in the classical and quantum experiments, particularly those pertaining to communication.

## SUPPLEMENTARY MATERIAL

See the [supplementary material](#) for supporting information.

## ACKNOWLEDGMENTS

I.N. and B.S. would like to acknowledge the Department of Science and Technology (South Africa) for funding and A.V. from the Claude Leon Foundation, F.C. is supported by funding from the Air Force Office of Scientific Research (Grant Nos. MURI: FA9550-14-1-0389, FA9550-16-1-0156), and the King Abdullah University of Science and Technology (KAUST) Office of Sponsored Research (OSR) (Award No. OSR-2016-CRG5-2995). Y.-W.H. and C.-W.Q. are supported by the National Research Foundation, Prime Minister’s Office, Singapore under its Competitive Research Program (CRP Award No. NRF-CRP15-2015-03). This work was performed, in part, at the Center for Nanoscale Systems (CNS), a member of the National Nanotechnology Coordinated Infrastructure (NNCI), which is supported by the NSF under Award No. 1541959. CNS is a part of Harvard University.

## DATA AVAILABILITY

The data that support the findings of this study are available from the corresponding author upon reasonable request.

## REFERENCES

- 1 L. Allen, M. W. Beijersbergen, R. Spreeuw, and J. Woerdman, “Orbital angular momentum of light and the transformation of Laguerre-Gaussian laser modes,” *Phys. Rev. A* **45**, 8185 (1992).
- 2 N. Heckenberg, R. McDuff, C. Smith, and A. White, “Generation of optical phase singularities by computer-generated holograms,” *Opt. Lett.* **17**, 221–223 (1992).
- 3 H. He, M. E. J. Friese, N. R. Heckenberg, and H. Rubinsztein-Dunlop, “Direct observation of transfer of angular momentum of absorptive particles from a laser beam with a phase singularity,” *Phys. Rev. Lett.* **75**, 826–829 (1995).
- 4 A. Mair, A. Vaziri, G. Weihs, and A. Zeilinger, “Entanglement of the orbital angular momentum states of photons,” *Nature* **412**, 313–316 (2001).
- 5 A. V. Carpentier, H. Michinel, J. R. Salgueiro, and D. Olivieri, “Making optical vortices with computer-generated holograms,” *Am. J. Phys.* **76**, 916–921 (2008).
- 6 E. Bolduc, N. Bent, E. Santamato, E. Karimi, and R. W. Boyd, “Exact solution to simultaneous intensity and phase encryption with a single phase-only hologram,” *Opt. Lett.* **38**, 3546–3549 (2013).
- 7 L. Marrucci, C. Manzo, and D. Paparo, “Optical spin-to-orbital angular momentum conversion in inhomogeneous anisotropic media,” *Phys. Rev. Lett.* **96**, 163905 (2006).
- 8 E. Brasselet, N. Murazawa, H. Misawa, and S. Juodkazis, “Optical vortices from liquid crystal droplets,” *Phys. Rev. Lett.* **103**, 103903 (2009).
- 9 J. Kim, Y. Li, M. N. Miskiewicz, C. Oh, M. W. Kudenov, and M. J. Escuti, “Fabrication of ideal geometric-phase holograms with arbitrary wavefronts,” *Optica* **2**, 958–964 (2015).
- 10 R. C. Devlin, A. Ambrosio, N. A. Rubin, J. P. B. Mueller, and F. Capasso, “Arbitrary spin-to-orbital angular momentum conversion of light,” *Science* **358**, 896–901 (2017).
- 11 M. Rafayelyan and E. Brasselet, “Laguerre–Gaussian modal q-plates,” *Opt. Lett.* **42**, 1966–1969 (2017).
- 12 M. Rafayelyan, T. Gertus, and E. Brasselet, “Laguerre-Gaussian quasi-modal q-plates from nanostructured glasses,” *Appl. Phys. Lett.* **110**, 261108 (2017).
- 13 M. J. Padgett, “Orbital angular momentum 25 years on,” *Opt. Express* **25**, 11265–11274 (2017).
- 14 H. Rubinsztein-Dunlop, A. Forbes, M. V. Berry, M. R. Dennis, D. L. Andrews, M. Mansuripur, C. Denz, C. Alpmann, P. Banzer, T. Bauer, E. Karimi, L. Marrucci, M. Padgett, M. Ritsch-Marte, N. M. Litchinitser, N. P. Bigelow, C. Rosales-Guzmán, A. Belmonte, J. P. Torres, T. W. Neely, M. Baker, R. Gordon, A. B. Stilgoe, J. Romero, A. G. White, R. Fickler, A. E. Willner, G. Xie, B. McMorrán, and A. M. Weiner, “Roadmap on structured light,” *J. Opt.* **19**, 013001 (2017).
- 15 A. E. Willner, H. Huang, Y. Yan, Y. Ren, N. Ahmed, G. Xie, C. Bao, L. Li, Y. Cao, Z. Zhao, J. Wang, M. P. J. Lavery, M. Tur, S. Ramachandran, A. F. Molisch, N. Ashrafi, and S. Ashrafi, “Optical communications using orbital angular momentum beams,” *Adv. Opt. Photonics* **7**, 66–106 (2015).
- 16 G. C. G. Berkhout, M. P. J. Lavery, J. Courtial, M. W. Beijersbergen, and M. J. Padgett, “Efficient sorting of orbital angular momentum states of light,” *Phys. Rev. Lett.* **105**, 153601 (2010).
- 17 F. Bouchard, N. H. Valencia, F. Brandt, R. Fickler, M. Huber, and M. Malik, “Measuring azimuthal and radial modes of photons,” *Opt. Express* **26**, 31925–31941 (2018).
- 18 E. Karimi, G. Zito, B. Piccirillo, L. Marrucci, and E. Santamato, “Hypergeometric-Gaussian modes,” *Opt. Lett.* **32**, 3053–3055 (2007).
- 19 B. Sephton, A. Dudley, and A. Forbes, “Revealing the radial modes in vortex beams,” *Appl. Opt.* **55**, 7830–7835 (2016).
- 20 D. Naidoo, F. S. Roux, A. Dudley, I. Litvin, B. Piccirillo, L. Marrucci, and A. Forbes, “Controlled generation of higher-order poincaré sphere beams from a laser,” *Nat. Photonics* **10**, 327–332 (2016).
- 21 H. Sroor, Y.-W. Huang, B. Sephton, D. Naidoo, A. Vallés, V. Ginis, C.-W. Qiu, A. Ambrosio, F. Capasso, and A. Forbes, “High-purity orbital angular momentum states from a visible metasurface laser,” *Nat. Photonics* (published online 2020).
- 22 V. D’ambrosio, N. Spagnolo, L. Del Re, S. Slussarenko, Y. Li, L. C. Kwek, L. Marrucci, S. P. Walborn, L. Aolita, and F. Sciarrino, “Photonic polarization gears for ultra-sensitive angular measurements,” *Nat. Commun.* **4**, 2432 (2013).
- 23 R. Fickler, G. Campbell, B. Buchler, P. K. Lam, and A. Zeilinger, “Quantum entanglement of angular momentum states with quantum numbers up to 10,010,” *Proc. Natl. Acad. Sci. U. S. A.* **113**, 13642–13647 (2016).
- 24 S. R. Nersisyan, N. V. Tabiryan, D. M. Steeves, and B. R. Kimball, “The promise of diffractive waveplates,” *Opt. Photonics News* **21**, 40–45 (2010).
- 25 R. Fickler, R. Lapkiewicz, W. N. Plick, M. Krenn, C. Schaeff, S. Ramelow, and A. Zeilinger, “Quantum entanglement of high angular momenta,” *Science* **338**, 640–643 (2012).
- 26 H. Qassim, F. M. Miatto, J. P. Torres, M. J. Padgett, E. Karimi, and R. W. Boyd, “Limitations to the determination of a Laguerre–Gauss spectrum via projective, phase-flattening measurement,” *J. Opt. Soc. Am. B* **31**, A20–A23 (2014).
- 27 G. Vallone, “Role of beam waist in Laguerre–Gauss expansion of vortex beams,” *Opt. Lett.* **42**, 1097–1100 (2017).
- 28 B. Sang, Y. Ke, J. Wu, H. Luo, W. Shu, and S. Wen, “Generation of pure Laguerre-Gaussian vector beams on the higher-order poincaré sphere by hollow Gaussian beams through dielectric metasurfaces,” *Opt. Commun.* **439**, 27–33 (2019).
- 29 N. Matsumoto, T. Ando, T. Inoue, Y. Ohtake, N. Fukuchi, and T. Hara, “Generation of high-quality higher-order Laguerre-Gaussian beams using liquid-crystal-on-silicon spatial light modulators,” *J. Opt. Soc. Am. A* **25**, 1642–1651 (2008).
- 30 T. Ando, Y. Ohtake, N. Matsumoto, T. Inoue, and N. Fukuchi, “Mode purities of Laguerre–Gaussian beams generated via complex-amplitude modulation using phase-only spatial light modulators,” *Opt. Lett.* **34**, 34–36 (2009).

- <sup>31</sup>S. Franke-Arnold, S. M. Barnett, M. J. Padgett, and L. Allen, “Two-photon entanglement of orbital angular momentum states,” *Phys. Rev. A* **65**, 033823 (2002).
- <sup>32</sup>J. Svozilik, J. Peřina, Jr., and J. P. Torres, “High spatial entanglement via chirped quasi-phase-matched optical parametric down-conversion,” *Phys. Rev. A* **86**, 052318 (2012).
- <sup>33</sup>M. Krenn, M. Huber, R. Fickler, R. Lapkiewicz, S. Ramelow, and A. Zeilinger, “Generation and confirmation of a (100× 100)-dimensional entangled quantum system,” *Proc. Natl. Acad. Sci. U. S. A.* **111**, 6243–6247 (2014).
- <sup>34</sup>J. Torres, A. Alexandrescu, and L. Torner, “Quantum spiral bandwidth of entangled two-photon states,” *Phys. Rev. A* **68**, 050301 (2003).
- <sup>35</sup>C. Law and J. Eberly, “Analysis and interpretation of high transverse entanglement in optical parametric down conversion,” *Phys. Rev. Lett.* **92**, 127903 (2004).
- <sup>36</sup>M. Agnew, J. Leach, M. McLaren, F. S. Roux, and R. W. Boyd, “Tomography of the quantum state of photons entangled in high dimensions,” *Phys. Rev. A* **84**, 062101 (2011).
- <sup>37</sup>A. Jesacher, C. Maurer, A. Schwaighofer, S. Bernet, and M. Ritsch-Marte, “Near-perfect hologram reconstruction with a spatial light modulator,” *Opt. Express* **16**, 2597–2603 (2008).
- <sup>38</sup>S. Choudhary, R. Sampson, Y. Miyamoto, O. S. Magaña-Loaiza, S. M. H. Rafsanjani, M. Mirhosseini, and R. W. Boyd, “Measurement of the radial mode spectrum of photons through a phase-retrieval method,” *Opt. Lett.* **43**, 6101–6104 (2018).